

neering at the Research Institute of Applied Electricity, Hokkaido University, Hokkaido, Japan. His principal fields of interest are measurement and control in the biomedical field, especially, microprocessor application to the medical instrumentation and the physiological experiments, and analysis of the neural activities and modeling of the neural network.

Dr. Hoshimiya is a member of the Institute of Electronics and Communication Engineers of Japan, the Japan Society of Medical Electronics and Biological Engineering, the Society of Instrument and Control Engineers of Japan, the Japan Neuroscience Society, and the Physiological Society of Japan.



Hachiro Inomata was born in Itoigawa, Japan, on December 18, 1933. He received the M.D. degree from Tohoku University, Sendai, Japan, in 1967.

From 1971 to 1974, he was a Research Associate in the Department of Pharmacology, State University of New York. He is presently an Associate Professor in the Department of Applied Physiology, School of Medicine, Tohoku University. His interests are voltage and patch clamp studies on muscle cells.

Dr. Inomata is a member of the Physiological Society of Japan and the Japan Society of Medical Electronics and Biological Engineering.

Pole-Zero Modeling and Classification of Phonocardiograms

TAE H. JOO, STUDENT MEMBER, IEEE, JAMES H. McCLELLAN, SENIOR MEMBER, IEEE, RODNEY A. FOALE, GORDON S. MYERS, AND ROBERT S. LEES

Abstract—Phonocardiography, the analysis of heart sounds, is a non-invasive diagnostic method useful in studying heart valve function. Phonocardiograms (PCG's) of porcine prosthetic heart valves in the aortic position were analyzed by a parametric signal modeling method in order to derive frequency domain features suitable for the classification of the valve state.

The Steiglitz-McBride method of pole-zero modeling was used to model the PCG's efficiently. The model gives a high-resolution spectral estimate from which the frequency domain features were derived.

The classification of PCG's was divided into two parts: feature selection and classification. The features selected for the classifier were the two maximum spectral peak locations. By assuming that the underlying probability density functions for the features are Gaussian, a quadratic Gaussian classifier was designed with a training set of 20 patients. The performance of the classifier was demonstrated by classifying a test set containing another 20 patients.

Manuscript received March 1, 1982; revised September 22, 1982. This work was supported by Grants from the Whitaker Health Science Foundation, the Pfeiffer Foundation, and the Ambrose Monell Foundation.

T. H. Joo was with the Research Laboratory of Electronics, Massachusetts Institute of Technology, Cambridge, MA 02139. He is now with the Laboratory for Information and Decision Systems, Massachusetts Institute of Technology, Cambridge, MA 02139.

J. H. McClellan was with the Research Laboratory of Electronics, Massachusetts Institute of Technology, Cambridge, MA 02139. He is now with Schlumberger, Austin Engineering Center, Austin, TX 78759.

R. A. Foale was with the Arteriosclerosis Center, Massachusetts Institute of Technology, Cambridge, MA 02139 and the Department of Medicine, Massachusetts General Hospital, Boston, MA 02114. He is now with the Department of Cardiology, Hammersmith Hospital, Royal Post Graduate Medical School, University of London, London, England.

G. S. Myers and R. S. Lees were with the Department of Medicine, Massachusetts General Hospital, Boston, MA 02114. They are now with the Arteriosclerosis Center, Massachusetts Institute of Technology, Cambridge, MA 02139 and the Department of Medicine, New England Deaconess Hospital, Boston, MA 02215.

I. INTRODUCTION

SIGNAL processing techniques have been applied to analyze biomedical signals such as the electrocardiogram, electroencephalogram, and phonocardiogram. One objective of signal analysis is to extract features of the signal that are useful for early detection of abnormalities. The topic of this paper is the analysis of phonocardiograms (PCG's) which are recordings of heart sounds. The Steiglitz-McBride method, an iterative pole-zero modeling method, is used to estimate the power spectrum of the PCG. The analysis yields spectral features for use in classifying patient PCG's as normal or abnormal to aid in clinical diagnosis. A Gaussian classifier was designed using a training set and then tested on 20 patients to study its performance.

The particular PCG's of interest were recorded from prosthetic heart valves which are used to replace severely damaged native heart valves. The most common prosthetic valve in use today is a porcine xenograft bioprosthesis (a pig aortic valve) [1]. These valves have been quite successful, but they are subject to problems of bacterial infection, paravalvular leakage, and limited durability. Our objective was to detect and possibly, to differentiate these problems through frequency analysis of the PCG.

Several diagnostic methods are available for detection of malfunctioning prosthetic valves. Existing techniques can be separated into invasive techniques, which make measurements inside the body, and noninvasive techniques, which operate external to the body. The noninvasive methods can be further divided into active methods, which transmit and receive a signal, and passive methods, which merely listen to signals gener-

ated by the heart. Because there is some risk associated with invasive techniques, noninvasive methods are preferred. Also, the noninvasive methods are more convenient and lend themselves to long term patient studies. On the other hand, non-invasive methods are limited somewhat in that they are of necessity indirect. Among the noninvasive methods, passive methods are simpler because no transmitter is required for signal generation; also, they are completely safe.

This paper is divided into five sections. In Section II, the nature of PCG's is discussed. Two important characteristics of the PCG data are emphasized. First, the length of the sound to be analyzed is approximately 20 ms. Hence, an FFT-based power spectrum estimator is limited in resolving close spectral peaks. This difficulty is circumvented by the Steiglitz-McBride method. Second, the heart sounds may vary in duration and amplitude from one beat to the next. Therefore, the spectral estimate must average several measurements. A multiple measurement version of the Steiglitz-McBride method is derived which averages the measurements in the correlation domain. In this section, a brief review of the previous work is also given.

In Section III, a summary of parametric modeling methods is given. The Steiglitz-McBride method is described in detail and the multiple measurement case is derived.

In Section IV, a classification algorithm for PCG's is given. First, feature selection is discussed. Heuristic features are selected from clinical observations and are measured from the power spectrum derived by the Steiglitz-McBride method. Using the features, a quadratic Gaussian classifier is designed from a training set which contains 20 patients. In Section V, the result of using the classifier on a test set of another 20 patients is discussed.

II. PHONOCARDIOGRAMS

This section describes the nature of the PCG signals. Two critical aspects of PCG data selection for analysis are examined. First, the signal of interest has short duration and must be separated from other sounds; second, the variation in the sound from one heart beat to the next requires some form of averaging.

A. Production of Phonocardiograms

Heart sounds originate when the major valves of the heart open and close and are believed to be caused primarily by the acceleration and deceleration of the blood mass and movements of the valves¹ [2, ch. 4]. The heart sounds contain two major components called the first heart sound and the second heart sound. The first heart sound complex may include closure of the mitral and tricuspid valves, vibrations from muscular contraction of the ventricles, opening of the pulmonary and aortic valves, and acceleration of blood into the pulmonary artery and the aorta. The entire first sound, including mitral and tricuspid components, lasts for an average of 100-120 ms in a normal adult.

The second heart sound occurs when the pulmonary and aortic valves close. The closure of the aortic valve (A_2) and the pulmonary valve (P_2) can often be separated in time; each component is approximately 10-30 ms in duration. The first

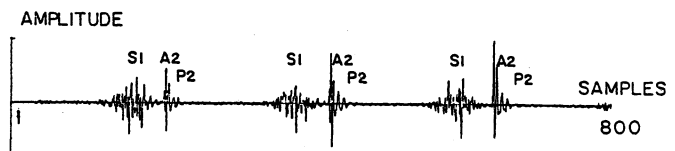


Fig. 1. Three cardiac cycles of abnormal aortic porcine valve PCG's.

and the second heart sounds are separated by approximately 300-400 ms.

The heart sounds vary significantly depending upon many factors including transducer location, impedance matching of the transducer/skin interface, respiration, and the position of the patient. The closing sound of the aortic valve can be recorded from several locations on the chest and the sound recording will vary depending upon the location. However, for the aortic valve analysis done here, recordings made from the second left sternal border were used exclusively. The transducer also involves a coupling effect because of the impedance mismatch between the receiver and the skin surface. In this study, a Hewlett-Packard heart sound transducer was used because the skin coupling to the transducer had a flat frequency response in the frequency range of interest [3]. The recording was made in held expiration to minimize any variation introduced by breathing.

B. Phonocardiogram Data Selection

The above considerations apply not only to normal aortic valves, but also to porcine prostheses in the aortic position. The rest of this paper is concerned with the analysis of the aortic closing sound of porcine prosthesis. Changes in integrity of aortic valve leaflets have been shown to affect this component of the heart sound [4]. Work by Stein [5] indicated that A_2 is directly related to vibrations of the valve leaflets upon closure. Also, the frequency spectrum of A_2 is modified by changes in the physical state of the valve [6], [7, pp. 167-174]. Therefore, examination of A_2 should give important information with which to classify the state of the valve.

From the entire PCG, an appropriate aortic closing sound must be selected by windowing in order to exclude other heart sounds. The exact location and the length of the data window are critical. Data selection is complicated further by a need to examine sounds from more than one cardiac cycle. The need to analyze multiple signals arises frequently in biomedical signal analysis because the underlying system is not stationary (i.e., all closing sounds are not exactly the same).

Fig. 1 shows three cardiac cycles from an abnormal aortic porcine valve. Two observations may be made from Fig. 1: first, A_2 's differ from one cycle to the next, and second, A_2 's are not always well separated from P_2 's. Ideally, A_2 should be isolated from P_2 in order to obtain a good spectral estimate. In practice, this is not always possible. However, satisfactory data selection can be accomplished by a user experienced in phonocardiography; here, the data selection was done by an experienced cardiologist. Even so, it is expedient to adopt the following rule for locating the time-sampling window: the beginning was defined such that the background noise (i.e., the low-amplitude component prior to A_2) was excluded; the end had to be estimated such that most of P_2 was excluded. This rule assumes that P_2 follows A_2 , which is usually the case. However, if P_2 precedes A_2 , the rule must

¹ The author would like to thank Dr. Charles W. Steiglitz for his help in this discussion. This work was supported in part by grants from the National Science Foundation and the National Institutes of Health.

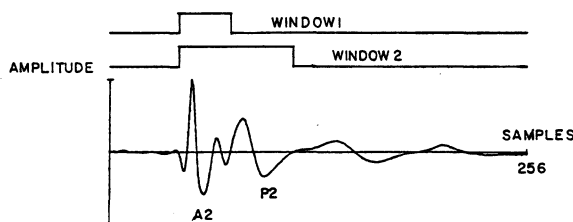


Fig. 2. Closing sound of porcine valve: two different window lengths. Window 1 is 34 points long and window 2 is 70 points long.

be modified accordingly. In a small number of cases, it is impossible to distinguish A_2 and P_2 in which case it could not be analyzed.

Two windows of lengths 34 and 70 points were used as indicated in Fig. 2. Fig. 3 demonstrates the effect of including P_2 in the spectral estimate. Fig. 3(a) shows that the power spectrum of the data selected by window 1 has one dominant peak. The spectrum of the data selected by window 2 [Fig. 3(b)] has multiple peaks in the lower frequency. Window 2 contains the pulmonary component of the closing sound and introduces an increase in the low-frequency component of the power spectrum.

After windowing the data from several cardiac cycles, multiple closing sounds must be time aligned. Two signals are time aligned by maximizing the cross correlation between them. For example, let $x(n)$ and $y(n)$ be two data measurements. Then, $y(n)$ must be shifted m units so that $\sum_n x(n)y(n+k)$ is a maximum for $k = m$. This operation, which must be carried out on several closing sounds, is implemented by a computer.

C. Previous Work

Analysis of PCG's in the time domain [8, pp. 443-457], [9, pp. 421-442], [10] and in the frequency domain [11], [12] have been described in previous research. In the time domain, parameters such as the timing of the sound with respect to the electrocardiogram and amplitude variation of the sound have been examined. In the frequency domain, features of the power spectrum such as the location of maximum peak have been used to indicate whether the valve is normal or abnormal. For example, changes in the frequency content of PCG's from abnormal mitral and aortic bioprosthetic valves were described by Stein *et al.* [13], [14], who reported that the PCG of an abnormal valve has more high-frequency content than that of a normal valve.

III. MODELING OF PHONOCARDIOGRAMS

In this section, several popular methods of signal modeling are reviewed. The discussion concentrates mainly on the Steiglitz-McBride algorithm for pole-zero modeling. A version that employs averaging over several cardiac cycles is also derived. This particular technique gives excellent frequency domain resolution while maintaining a faithful time domain match to the original data. Therefore, this estimator was chosen to derive the spectral features for classification (Section IV).

A. Parametric Signal Modeling Methods

Power spectrum estimation can be performed by modeling a signal in the following way. Consider the system $H(z)$ having a rational z -transform

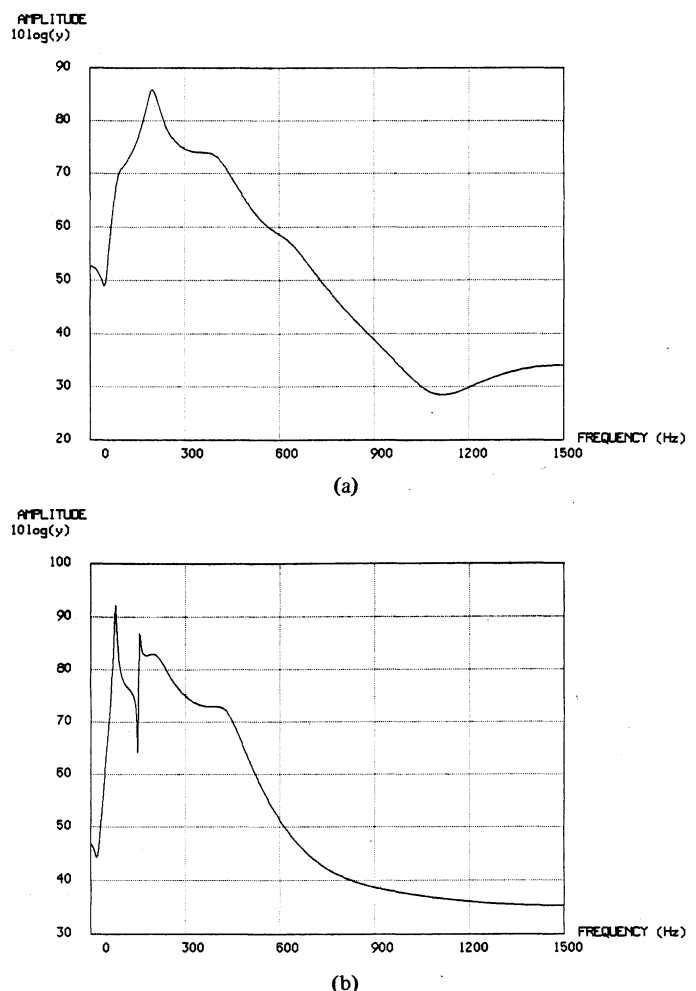


Fig. 3. (a) Spectrum of window 1 estimated by the Steiglitz-McBride method. (b) Spectrum of window 2 estimated by the Steiglitz-McBride method.

$$H(z) = \frac{B(z)}{A(z)} \quad (1)$$

where

$$A(z) = 1 + \sum_{k=1}^P a_k z^{-k}$$

and

$$B(z) = \sum_{k=0}^Q b_k z^{-k}.$$

If the parameters $\{a_k\}$ and $\{b_k\}$ are chosen so that the impulse response of (1) $h(n)$ approximates the given signal $s(n)$, then the power spectrum of $s(n)$ can be taken to be $|B(e^{j2\pi f})|^2 / |A(e^{j2\pi f})|^2$. Experience has shown that this approach to power spectrum estimation can yield very high resolution of narrowband signals. One well-known estimator of this type is the maximum entropy method (MEM) developed by Burg [15]. For MEM, the numerator of (1) is a constant; the frequency domain resolution is attractive, but the time-domain match is not always acceptable.

One viewpoint that helps to explain the high-resolution capability of (1) is obtained by examining the time-domain form of $H(z)$. In the time domain, $s(n)$ is approximated by

$$\sum_{k=1}^P a_k e^{-jnT_k}, \quad n \geq 0 \quad (2)$$

where the parameters $\{c_k\}$ and $\{T_k\}$ are obtained easily from $\{a_k\}$ and $\{b_k\}$. In particular, the exponentials e^{T_k} are the roots of $A(z) = 0$. In contrast to (2), an FFT estimator would expand the signal as

$$s(n) = \sum_{k=0}^{N-1} S_k e^{j(2\pi/N)nk} \quad (3)$$

where $\{S_k; k = 0, \dots, N-1\}$ is the FFT of $\{s(n); n = 0, \dots, N-1\}$. The power of signal modeling comes from the fact that the exponentials are chosen (optimally) for a particular signal, whereas the FFT uses fixed complex exponentials independent of the nature of the signal. Furthermore, the number of exponentials needed to model a signal accurately can be quite small and again, the FFT always uses N exponentials where N is equal to the length of the signal $s(n)$. Obviously, this modeling approach is attractive when the signal is well represented by a few exponentials which seems to be the case for PCG's [16].

There are quite a few distinct methods for calculating the parameters of the model in (1). An obvious approach is to minimize the energy in the error between $h(n)$ and $s(n)$

$$E = \sum_{n=0}^{\infty} |h(n) - s(n)|^2. \quad (4)$$

This least-squares minimization problem is, unfortunately, nonlinear and difficult to solve. Many existing modeling methods solve instead a linear mean-square problem that minimizes a modified error energy [17]. The most successful of these are the all-pole (or autoregressive) methods. Examples include the autocorrelation and covariance methods of linear prediction [18]. MEM spectrum analysis also falls in this category. All-pole models are somewhat restrictive and so there has been an effort to compute pole-zero models. Among these pole-zero (or ARMA-autoregressive moving average) techniques are Prony's method [19], Padé's approximation [20], [21], Shanks' method [22], Kalman's method [23], and the Steiglitz-McBride iteration [24]. Of these, only the last seeks to minimize the error measure of (4) and hence, it should lead to the best model of the signal.

A comparison of different modeling methods on the basis of time-domain error shows the superiority of the Steiglitz-McBride method. Specifically, consider the normalized error measure

$$\text{NMSE} \equiv \frac{\left[\sum_{n=0}^{N-1} |h(n) - s(n)|^2 \right]^{1/2}}{\left[\sum_{n=0}^{N-1} |s(n)|^2 \right]^{1/2}}. \quad (5)$$

Several methods were applied to the data selected by Window 1 of Fig. 2. The NMSE of the Steiglitz-McBride model is 0.078, for Shanks' model it is 0.166, and for Kalman's model it is 0.611. The NMSE of the all-pole autocorrelation model is 1.62 and the covariance model is 1.08.

This result is in agreement with that reported by Steiglitz on speech data [25]. In general, the pole-zero methods perform better than the all-pole methods in matching the input signal because they are not constrained to be minimum phase systems and the numerator of the model is not constrained to be

constant. The Steiglitz-McBride method performs better than the other pole-zero methods because it seeks to minimize (4). In the next section, the Steiglitz-McBride method is explained in some detail and the method is extended to include multiple measurements of the signal to be modeled.

B. Multiple Measurement Steiglitz-McBride Method

The Steiglitz-McBride method is an iterative algorithm for computing a model. This method was originally formulated as a system identification technique given input and output data. However, the impulse-input case is important for signal modeling. The error energy in (4) can be rewritten as

$$E = \sum_{n=0}^{N-1} \left| \frac{1}{A} [A[s(n)] - B[\delta(n)]] \right|^2 \quad (6)$$

where $A[\cdot]$ and $B[\cdot]$ are the convolutional operators for $A(z)$ and $B(z)$, respectively. ($1/A$ is the operator for the inverse system $1/A(z)$.) Assume $A_{i-1}(z)$, an estimate of $A(z)$ at the $i-1$ th iteration, is given; then, (6) can be modified as

$$\tilde{E}^{(i)} = \sum_{n=0}^{N-1} \left| \frac{1}{A_{i-1}} [A_i[s(n)] - B_i[\delta(n)]] \right|^2 = \sum_{n=0}^{N-1} |\tilde{e}^{(i)}(n)|^2 \quad (7a)$$

where

$$\begin{aligned} \tilde{e}^{(i)}(n) &= A_i \left[\frac{1}{A_{i-1}} [s(n)] \right] - B_i \left[\frac{1}{A_{i-1}} [\delta(n)] \right] \\ &= A_i[\tilde{s}(n)] - B_i[\tilde{x}(n)]. \end{aligned} \quad (7b)$$

In other words, after $s(n)$ and $\delta(n)$ are filtered by $1/A_{i-1}(z)$, the error is linear in the coefficients of A_i and B_i and the minimization of (7) is straightforward. The solution that minimizes (4) is obtained by iterating (7) until $A_i(z)$ is very close to $A_{i-1}(z)$. If convergence occurs, the error in (7a) is equal to the true error in (4) and the solution will be very close to the correct answer [24]. Experience shows that only a few iterations are necessary to reduce the error of (4) significantly, but there is no theoretical proof of convergence except for the case of infinitely long data [26].

For the single input case, the error to minimize for the i th iteration is given by (7). $\tilde{E}^{(i)}$ is maximized at a stationary point of the derivative to obtain

$$\begin{aligned} \frac{\partial \tilde{E}^{(i)}}{\partial a_k} &= 2 \sum_{n=0}^{N-1} \tilde{e}^{(i)}(n) \frac{\partial \tilde{e}^{(i)}(n)}{\partial a_k} = \sum_{n=0}^{N-1} \tilde{s}(n-i) \tilde{e}^{(i)}(n) = 0 \\ \frac{\partial \tilde{E}^{(i)}}{\partial b_j} &= 2 \sum_{n=0}^{N-1} \tilde{e}^{(i)}(n) \frac{\partial \tilde{e}^{(i)}(n)}{\partial b_j} = \sum_{n=0}^{N-1} \tilde{x}(n-j) \tilde{e}^{(i)}(n) = 0 \end{aligned} \quad (8)$$

for $k = 1, 2, \dots, P$ and $j = 0, 1, \dots, Q$. By replacing $\tilde{e}^{(i)}(n)$ in (8) with (7b), the following normal equations result.

$$\begin{bmatrix} \mathbf{u} \\ \mathbf{v} \end{bmatrix} = \begin{bmatrix} \Phi_{\tilde{x}\tilde{x}} & \Phi_{\tilde{s}\tilde{x}}^T \\ \Phi_{\tilde{s}\tilde{x}} & \Phi_{\tilde{s}\tilde{s}} \end{bmatrix} \begin{bmatrix} \mathbf{b} \\ -\mathbf{a} \end{bmatrix} \quad (9)$$

$$\mathbf{u}^T = [\phi_{\tilde{s}\tilde{x}}(0, 0) \phi_{\tilde{s}\tilde{x}}(0, 1) \cdots \phi_{\tilde{s}\tilde{x}}(0, Q)]$$

$$\mathbf{v}^T = [\phi_{\tilde{s}\tilde{s}}(0, 1) \phi_{\tilde{s}\tilde{s}}(0, 2) \cdots \phi_{\tilde{s}\tilde{s}}(0, P)]$$

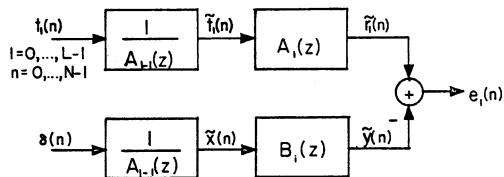


Fig. 4. Multiple measurement Steiglitz-McBride method.

with

$$\begin{aligned}\Phi_{\tilde{s}\tilde{s}} &= [\phi_{\tilde{s}\tilde{s}}(k, j)] \quad \text{for } k = 1, \dots, P \text{ and } j = 1, \dots, P \\ \Phi_{\tilde{s}\tilde{x}} &= [\phi_{\tilde{s}\tilde{x}}(k, j)] \quad \text{for } k = 1, \dots, P \text{ and } j = 0, \dots, Q \\ \Phi_{\tilde{x}\tilde{x}} &= [\phi_{\tilde{x}\tilde{x}}(k, j)] \quad \text{for } k = 0, \dots, Q \text{ and } j = 0, \dots, Q\end{aligned}$$

where

$$\phi_{fg}(k, j) \equiv \sum_{n=0}^{N-1} f(n-k) g(n-j).$$

The coefficient matrix in (9) is positive semidefinite. In practice, this matrix is usually positive definite, in which case the Cholesky decomposition can be used to solve the linear equations efficiently.

For the multiple measurement case, a different error criterion must be employed. One extension of the single measurement case is presented here. Assume L measurements of N points each are given $\{s_l(n): l = 0, 1, \dots, L-1 \text{ and } n = 0, 1, \dots, N-1\}$. Each of the L measurements does not necessarily have to be the same length. However, the derivation for the variable measurement length case is identical to the equal length case; hence, the same length is assumed for all measurements to simplify the notation. To generalize the derivation, N would merely be replaced by N_l for the l th measurement. Given the multiple measurements, a new set of signals is defined by scaling each measurement as $t_l(n) = \gamma_l s_l(n)$ for $l = 0, 1, \dots, L-1$ and $n = 0, 1, \dots, N-1$, where γ_l is the gain factor for each segment defined as

$$\gamma_l = \frac{\text{total energy}}{\text{energy in } l\text{th measurement}} = \frac{\left[\frac{1}{L} \sum_{l=0}^{L-1} \sum_{n=0}^{N-1} s_l^2(n) \right]^{1/2}}{\left[\sum_{n=0}^{N-1} s_l^2(n) \right]^{1/2}}. \quad (10)$$

The new modified error to be minimized at the i th iteration is defined now as

$$\tilde{E}_{\text{new}}^{(i)} = \frac{1}{L} \sum_{l=0}^{L-1} \sum_{n=0}^{N-1} |e_l(n)|^2,$$

where $e_l(n) = \tilde{r}_l(n) - \tilde{y}(n)$ (see Fig. 4).

The resulting normal equations are in the same form as in (9), but the entries in the matrices involve some averaging.

$$\begin{aligned}\mathbf{u}^T &= \left[\sum_{l=0}^{L-1} \gamma_l \phi_{\tilde{s}\tilde{x}}(0, 0) \sum_{l=0}^{L-1} \gamma_l \phi_{\tilde{s}\tilde{x}}(0, 1) \cdots \sum_{l=0}^{L-1} \gamma_l \phi_{\tilde{s}\tilde{x}}(0, Q) \right] \\ \mathbf{v}^T &= \left[\sum_{l=0}^{L-1} \gamma_l \phi_{\tilde{s}\tilde{s}}(0, 1) \sum_{l=0}^{L-1} \gamma_l \phi_{\tilde{s}\tilde{s}}(0, 2) \cdots \sum_{l=0}^{L-1} \gamma_l \phi_{\tilde{s}\tilde{s}}(0, P) \right]\end{aligned}$$

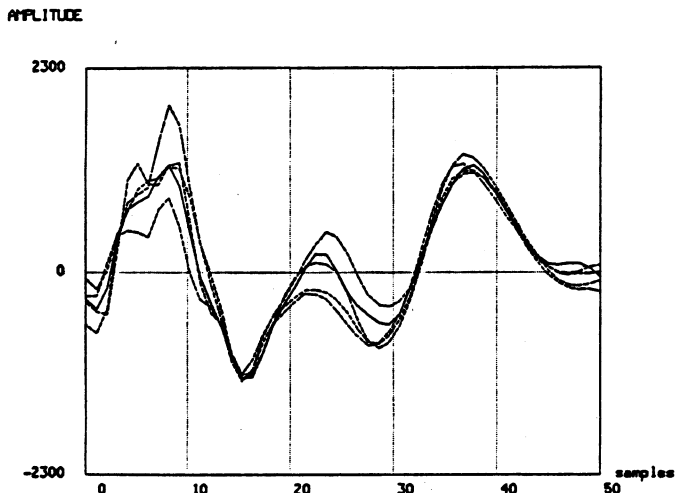


Fig. 5. Four aortic porcine valve closing sounds (dotted line) and the impulse response of the Steiglitz-McBride model (solid line).

with

$$\Phi_{\tilde{s}\tilde{s}} = \left[\sum_{l=0}^{L-1} \gamma_l^2 \phi_{\tilde{s}\tilde{s}}(i, j) \right]$$

$$\Phi_{\tilde{s}\tilde{x}} = \left[\sum_{l=0}^{L-1} \gamma_l \phi_{\tilde{s}\tilde{x}}(i, j) \right]$$

$$\Phi_{\tilde{x}\tilde{x}} = \left[\sum_{l=0}^{L-1} \phi_{\tilde{x}\tilde{x}}(i, j) \right].$$

Since γ_l is a positive constant, the positive semidefiniteness property of the single measurement case also holds true for this case; in practice, the matrix is almost always invertible. For the analysis of PCG's, the Steiglitz-McBride method has been used successfully with $P = 8$ and $Q = 8$ on four segments of data, each approximately 80 points long. Five iterations of the algorithm are usually sufficient to obtain a good model. Fig. 5 shows an example of the time-domain match of the model. Four aortic porcine valve closings, indicated by the dotted lines, are used to determine the multiple measurement Steiglitz-McBride model with $P = 8$, $Q = 8$, and 5 iterations. The impulse response of the model, indicated by the solid line, demonstrates an excellent match. In the next section, the power spectrum derived from the model is used to design a classification scheme based on spectral features.

IV. CLASSIFICATION OF PHONOCARDIOGRAMS

In this section, the classification of porcine prosthetic valves into normal or abnormal by spectrum analysis of the phonocardiogram is discussed. The approach taken here is based on pattern recognition. As such, it is separated into two steps: feature selection and classifier design. Spectral peaks from a parametric model are shown to be effective features and a classifier is designed assuming that the underlying probability density functions are Gaussian. First, a rationale is given for the features selected. Because spectral peaks are used for classification, the Steiglitz-McBride model is used to obtain the spectral estimate. Then, a Gaussian classifier is designed based on a training set of 20 patients.

A. Feature Selection

A heuristic method of feature selection may be based on a model of the sound-production process. When a physical model is not available, an understanding of the signal generation process may be used to select the feature vector. One drawback of this approach is that many different feature vectors are available and the optimum one cannot be determined. The usefulness of the heuristic feature vector can only be measured by its performance in classifying test data.

Cardiologists use the sounds heard through the stethoscope to diagnose the state of patients' heart valves. One key characteristic cardiologists use is frequency content; thus, the power spectrum is an effective domain in which to extract features.

An increase in high-frequency energy with aging and degeneration of porcine valves was reported by Stein *et al.* [14]; our preliminary observations are in agreement with these data. However, the increase in peak location reported by Stein *et al.* is based on FFT analysis which does not resolve secondary peaks in the spectrum and introduces power leakage through the sidelobes. Our data show that the resonant peak locations in the power spectrum and their relative energy correlate well with the state of the valve. The heuristic feature vector selected for classification in this study contains the two maximum peak locations, i.e., $\mathbf{x} = [f_1 \ f_2]$, where f_1 and f_2 are the locations of the two maximum peaks and the power at f_1 is greater than the power at f_2 . The power under each peak must be estimated as the product of the peak spectral amplitude and the 3 dB bandwidth, where the 3 dB bandwidth is approximated from the spectrum. This is the usual procedure in MEM and other high-resolution spectral estimators [27]. The next section considers the design of a classifier based on f_1 and f_2 .

B. Classifier Design

The design of a classifier is based on a statistical model for the dependence of the peak frequencies upon the state of the valve. For PCG analysis, the probability density functions (PDF's) are assumed to be known because a test set can be used to estimate the PDF's. The classifier with the minimum probability of error is called an optimum classifier and is determined by the *Bayes' likelihood ratio test*. Let C_n and C_a denote the normal and abnormal classes, respectively. The classifier derived by minimizing the Bayes' risk is

$$\text{if } P_{C_n|x}(C_n|x) \geq P_{C_a|x}(C_a|x), \text{ then decide } C_n$$

$$\text{if } P_{C_n|x}(C_n|x) \leq P_{C_a|x}(C_a|x), \text{ then decide } C_a$$

where \mathbf{x} denotes the feature vector. Using Bayes' rule and assuming the underlying PDF's are Gaussian, i.e., let $P_{\mathbf{x}|C_n}(\mathbf{x}|C_n)$ and $P_{\mathbf{x}|C_a}(\mathbf{x}|C_a)$ be Gaussian densities for the normal and abnormal with means \mathbf{m}_n and \mathbf{m}_a and covariances K_n and K_a , respectively, the discriminant function becomes

$$g(\mathbf{x}) = (\mathbf{x} - \mathbf{m}_a)^T K_a^{-1} (\mathbf{x} - \mathbf{m}_a) - (\mathbf{x} - \mathbf{m}_n)^T K_n^{-1} (\mathbf{x} - \mathbf{m}_n) + \ln \frac{|K_a|}{|K_n|} - 2 \ln \frac{P_{C_a}(C_a)}{P_{C_n}(C_n)} \quad (11)$$

which is a quadratic function of \mathbf{x} [28, pp. 33-69].

TABLE I
THE TRAINING SET USED TO DESIGN THE CLASSIFIER

Training Set		
Valve	f1(Hz)	f2(Hz)
normal#1	172.	79.
normal#2	140.	99.
normal#3	82.	114.
normal#4	84.	123.
normal#5	123.	155.
normal#6	90.	131.
normal#7	79.	137.
normal#8	134.	99.
normal#9	148.	102.
normal#10	111.	73.
normal#11	93.	73.
normal#12	96.	131.
normal#13	87.	143.
normal#14	125.	70.
average	121.	109.
abnormal#1	184.	257.
abnormal#2	158.	216.
abnormal#3	213.	87.
abnormal#4	193.	117.
abnormal#5	178.	290.
abnormal#6	131.	193.
average	176.	193.

The feature vector selected was used to design a classifier and the performance of the classifier was evaluated on a test set. Valve classification is a supervised parametric classification problem because a training set is available and the PDF's are assumed to be Gaussian. The training set consists of 20 patients, of which 14 were normal and 6 abnormal. The training set was defined through examination of clinical data by one or more cardiologists. The extracted feature vector and the estimated means are listed in Table I. The means and the variances are estimated by

$$\text{mean} = \bar{\mathbf{x}}^{(j)} = \frac{1}{N^{(j)}} \sum_{i=1}^{N^{(j)}} \mathbf{x}_i$$

and

$$K^{(j)} \equiv \frac{1}{N^{(j)}} \sum_{i=1}^{N^{(j)}} (\mathbf{x}_i - \bar{\mathbf{x}}^{(j)}) (\mathbf{x}_i - \bar{\mathbf{x}}^{(j)})^T$$

$j = n$ and a for normal and abnormal, respectively. As indicated by Table I, the means of the abnormal values are higher than those of the normal values: $\bar{\mathbf{x}}_n = [121 \ 109]$ and $\bar{\mathbf{x}}_a = [176 \ 193]$. Also, the abnormal valves have larger variances than the normal valves, especially for f_2 .

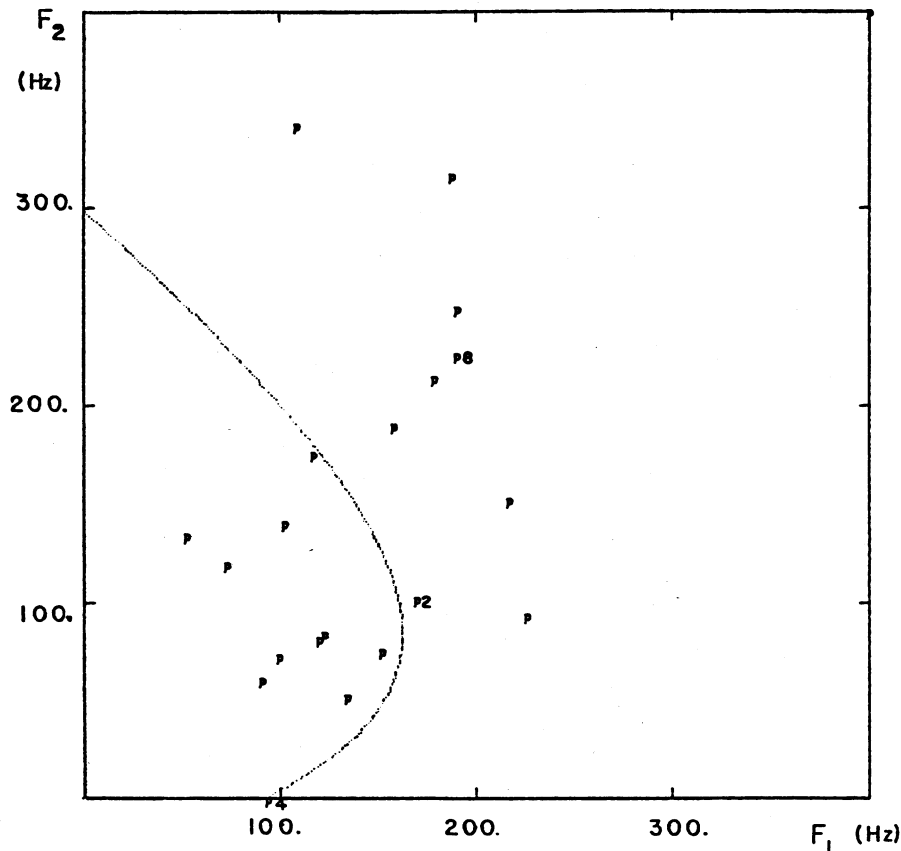


Fig. 6. Test set and the decision boundary in the feature space. Misclassified patients are Patients 2, 4, and 8. Refer to Table II for numerical values.

$$K_n = \begin{bmatrix} 775 & -359 \\ -359 & -756 \end{bmatrix}$$

and

$$K_a = \begin{bmatrix} 679 & -819 \\ -819 & 5162 \end{bmatrix}.$$

A Gaussian classifier is used to define a quadratic decision surface in the feature space. By using the estimated means and the variances, the Gaussian classifier was designed and the resulting discriminant function was

$$g(\mathbf{x}) = \begin{bmatrix} f_1 - 176 \\ f_2 - 193 \end{bmatrix}^T \begin{bmatrix} 1.81e-3 & 2.88e-4 \\ 2.88e-4 & 5.82e-10 \end{bmatrix} \begin{bmatrix} f_1 - 176 \\ f_2 - 193 \end{bmatrix} - \begin{bmatrix} f_1 - 121 \\ f_2 - 109 \end{bmatrix}^T \begin{bmatrix} 1.65e-3 & 7.85e-4 \\ 7.85e-4 & 1.69e-3 \end{bmatrix} \begin{bmatrix} f_1 - 121 \\ f_2 - 109 \end{bmatrix} + 1.82.$$

The decision boundary for this training set is a hyperbola in the feature space (see Fig. 6).

V. RESULTS AND CONCLUSIONS

In order to evaluate the performance of the above classifier, a test set which contained 20 additional patients, 13 normal and 7 abnormal, was classified. The test data were determined by a cardiologist using clinical data. Table II describes the test data and the outcome of the classification and the data are plotted in Fig. 6. The result of the classifier was compared to

TABLE II
TEST SET—OUTCOME OF THE CLASSIFIER AND THE CLINICAL DIAGNOSIS

patient#	Test Set				
	f1	f2	g(x)	classification	diagnosis
1	73.	120.	23.6	normal	normal
2	169.	102.	-2.68	abnormal	normal
3	120.	82.	10.2	normal	normal
4	93.	0.0	-0.45	abnormal	normal
5	52.	134.	29.4	normal	normal
6	123.	84.	9.64	normal	normal
7	134.	52.	4.14	normal	normal
8	190.	225.	-44.7	abnormal	normal
9	99.	73.	14.8	normal	normal
10	90.	61.	15.5	normal	normal
11	102.	140.	12.8	normal	normal
12	117.	175.	0.9	normal	normal
13	152.	76.	2.1	normal	normal
14	158.	190.	-17.9	abnormal	abnormal
15	218.	152.	-24.4	abnormal	abnormal
16	178.	213.	-34.7	abnormal	abnormal
17	225.	93.	-15.5	abnormal	abnormal
18	108.	342.	-85.8	abnormal	abnormal
19	190.	249.	-57.5	abnormal	abnormal
20	187.	318.	-103.	abnormal	abnormal

the clinical diagnosis; three clinically well patients are classified as abnormalities. Therefore, this classifier correctly classified 17 out of 20 patients, as indicated by Fig. 6. Two of the misclassified patients, Patients 2 and 4, were close to the decision boundary which is also indicated by the small $g(\mathbf{x})$ values in Table II. Patient 8 was clearly outside the putative normal area. According to this classifier, this valve should be clearly abnormal. Thus, Patient 8 caused the only serious disagreement between the classifier and the clinical diagnosis. However, all the misclassifications were false alarms (classifying normal as abnormal) which are considered by physicians to be less critical than misses (classifying abnormal as normal) in clinical applications since further and more definitive testing usually clarifies the diagnosis.

A. Summary

The data suggest that a simple signal processing algorithm may be useful in the diagnosis of prosthetic valve dysfunction. Based on clinical experience, a heuristic feature vector $\mathbf{x} = [f_1 \ f_2]$ where f_1 and f_2 are the locations of the two maximum frequency peaks such that the power at f_1 is greater than the power at f_2 was selected. The power spectrum of the closing sound of the aortic prosthetic valve was derived by the multiple measurement Steiglitz-McBride method. This feature vector was then used to design a Gaussian classifier. The classifier defines a hyperbola in the feature space to separate normal from abnormal. A training set of 20 patients was used to estimate the means and the covariances of the underlying probability density functions. The performance of the classifier was evaluated on the test set which contained another 20 patients. The classifier correctly classified 17 of these 20 patients, and only 1 of the 3 misclassified patients had a feature vector that was not near the decision boundary in the feature space. All the misclassified patients were false-alarm cases.

A large patient population will be needed to prove the effectiveness of the classification method described above. The accurate time domain match and high-resolution spectral estimate of the Steiglitz-McBride model are two primary advantages of this method. For this reason, our classification algorithm may be applicable to heart sounds in addition to the closing sound of the aortic valve.

REFERENCES

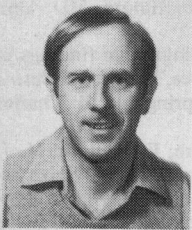
- [1] W. W. Angell and J. D. Angell, "Porcine valves," *Progr. Cardiovasc. Dis.*, vol. 23, pp. 141-166, 1980.
- [2] M. E. Tavel, *Clinical Phonocardiography and External Pulse Recording*, 3rd ed. Chicago IL: Times-Mirror, 1978.
- [3] J. J. Fredberg, personal communication.
- [4] H. N. Sabbah, F. Khaja, D. T. Anbe, G. M. Folger, and P. D. Stein, "Determinants of the amplitude of the aortic component of the second heart sound in aortic stenosis," *Amer. J. Cardiol.*, vol. 41, pp. 830-835, 1978.
- [5] P. D. Stein, *A Physical and Physiological Basis for the Interpretation of Cardiac Auscultation*. Mount Kisco, NY: Futura, 1981.
- [6] E. F. Blick, H. N. Sabbah, and P. D. Stein, "One dimensional model of diastolic semilunar valve vibration productive of heart sounds," *J. Biomech.*, vol. 12, pp. 223-227, 1979.
- [7] V. A. McKusick, *Cardiovascular Sound in Health and Disease*. Baltimore, MD: Williams and Wilkins, 1958.
- [8] G. Jacovella, P. Giampaolo, G. Gambelli, E. Giovannini, V. Rulli, and G. Chidichimo, "Phonocardiographic and echocardiographic diagnosis of prosthetic valve malfunction," in *Non-Invasive Cardiovascular Diagnosis*, E. B. Dietrich. Baltimore, MD: University Park Press, 1978.
- [9] O. Zoneraich and S. Zoneraich, "Phonocardiographic findings in patients with malfunctioning artificial valves," in *Non-Invasive Methods in Cardiology*, S. Zoneraich, Ed. Springfield, IL: Charles C Thomas, 1974.
- [10] J. T. Willerson, J. A. Kastor, R. E. Dinsmore, E. Mundth, M. J. Buckley, W. Gerald Austen, and C. Sanders, "Non-invasive assessment of prosthetic mitral paravalvular and intravalvular regurgitation," *Brit. Heart J.*, vol. 34, pp. 561-568, 1972.
- [11] B. Kingsley, "Acoustic evaluation of prosthetic cardiac valve in the audio spectrum," *J. Audio Eng. Soc.*, pp. 750-755, Nov. 1972.
- [12] R. F. Gordon, M. Najmi, B. Kingsley, B. L. Segal, and J. Linhart, "Spectroanalytic evaluation of aortic prosthetic valves," *Chest*, vol. 66, pp. 44-49, July 1974.
- [13] P. D. Stein, H. N. Sabbah, J. B. Lakier, D. J. Magilligan, Jr., and S. Goldstein, "Frequency of the first heart sound in the assessment of stiffening of mitral bioprosthetic valves," *Circulation*, vol. 63, pp. 200-203, 1981.
- [14] P. D. Stein, H. N. Sabbah, J. B. Lakier, and S. Goldstein, "Frequency spectrum of the aortic component of the second heart sound in patients with normal valves, aortic stenosis and aortic porcine xenografts," *Amer. J. Cardiol.*, vol. 46, pp. 48-52, July 1980.
- [15] J. P. Burg, "Maximum entropy spectral analysis," presented at the 37th S.E.G. Annu. Meet., Oklahoma City, OK, 1967.
- [16] T. H. Joo, "Pole-zero modeling and classification of phonocardiograms," M.S. thesis, Dept. Elec. Eng. and Comput. Sci., Massachusetts Inst. Technol., Cambridge, MA, Jan. 1982.
- [17] J. H. McClellan, "Parametric signal modelling notes," Dept. Elec. Eng. and Comput. Sci., Massachusetts Inst. Technol., Cambridge, MA, 1981.
- [18] J. Makhoul, "Linear prediction: A tutorial review," *Proc. IEEE*, vol. 63, pp. 561-580, Apr. 1974.
- [19] C. S. Burrus and T. W. Parks, "Time domain design of recursive digital filters," *IEEE Trans. Audio Electroacoust.*, vol. AU-18, pp. 137-141, June 1970.
- [20] F. Brophy and A. C. Salazar, "Recursive digital filter synthesis in the time domain," *IEEE Trans. Acoust., Speech, Signal Processing*, vol. ASSP-22, pp. 45-55, Feb. 1974.
- [21] R. Hasting-James and S. K. Mehra, "Extension of the padé-approximant technique for the design of recursive digital filters," *IEEE Trans. Acoust., Speech, Signal Processing*, vol. ASSP-25, pp. 501-509, Dec. 1977.
- [22] J. L. Shanks, "Recursive filters for digital processing," *Geophysics*, vol. 32, pp. 32-51, Feb. 1967.
- [23] R. E. Kalman, "Design of a self-optimizing control system," *Trans. ASME*, vol. 80, pp. 468-478, Feb. 1958.
- [24] K. Steiglitz and L. E. McBride, "A technique for the identification of linear systems," *IEEE Trans. Automat. Contr.*, vol. AC-10, pp. 461-464, Oct. 1965.
- [25] K. Steiglitz, "On the simultaneous estimation of poles and zeros in speech analysis," *IEEE Trans. Acoust., Speech, Signal Processing*, vol. ASSP-25, pp. 229-234, June 1977.
- [26] P. Stoica and T. Soderstrom, "The Steiglitz-McBride identification algorithm revisited—Convergence analysis and accuracy aspects," *IEEE Trans. Automat. Contr.*, vol. AC-26, pp. 712-717, June 1981.
- [27] R. T. Lacoss, "Data adaptive spectral analysis methods," *Geophysics*, vol. 36, pp. 661-675, Aug. 1971.
- [28] K. Fukunaga, *Introduction Statistical Pattern Recognition*. New York: Academic, 1972.



Tae H. Joo (S'82) was born in Seoul, South Korea, on November 18, 1958. He received the B.S. degree in electrical engineering from Georgia Institute of Technology, Atlanta, in 1980 and the M.S. degree from the Massachusetts Institute of Technology, Cambridge, in 1982.

He is presently with the Research Laboratory of Electronics, Massachusetts Institute of Technology.

Mr. Joo is a member of Tau Beta Pi and Eta Kappa Nu.



James H. McClellan (S'69-M'74-SM'79) was born in Guam on October 5, 1947. He received the B.S. degree in electrical engineering from Louisiana State University, Baton Rouge, in 1969, and the M.S. and Ph.D. degrees from William Marsh Rice University, Houston, TX, in 1972 and 1973, respectively.

From 1973 to 1975 he was a member of the Research Staff, Lincoln Laboratory, working on problems in radar signal processing. From 1975 to 1982 he was a Professor in the Department of Electrical Engineering, Massachusetts Institute of Technology, Cambridge, where he taught graduate courses in digital signal processing. He is now with Schlumberger, Austin Engineering Center, Austin, TX, where he is engaged in the application of signal processing to well-log data.



Rodney A. Foale received the M.B., B.S., and M.R.C.P. degrees from Melbourne University, Melbourne, Australia.

Since 1974 he has been a Resident in London, England, and has pursued active research in clinical cardiology, first at the National Heart Hospital and Cardiothoracic Institute of London, London, England, and then at Massachusetts General Hospital, Boston. He is now Senior Registrar in Cardiology at Hammersmith Hospital, Royal Post Graduate School, University of London, London, England.



Gordon S. Myers received the M.D. degree from Harvard Medical School, Cambridge, MA, in 1940.

He was an Intern and Resident at Massachusetts General Hospital, Boston, and then served in the U.S. Navy from 1944 to 1946. He then returned to Massachusetts General Hospital as a Research and Clinical Fellow in Cardiology. He is now an Associate Clinical Professor of Medicine at Harvard Medical School, Senior Physician at Massachusetts

General Hospital, a Research Affiliate at Massachusetts Institute of Technology, Cambridge, and an Associate Physician at New England Deaconess Hospital, Boston, MA.



Robert S. Lees received the M.D. degree from Harvard Medical School, Cambridge, MA, in 1959.

He was an Intern, Resident, and Research Fellow at Massachusetts General Hospital, Boston, before becoming a Fellow in Cardiology at the National Heart Hospital, London, England. After that, he spent three years at the National Heart Institute, Bethesda, MD. He is now Professor of Cardiovascular Disease at Massachusetts Institute of Technology, Cambridge, and Director of Medical Research at New England Deaconess Hospital, Boston, MA.

Current Pathways in High-Voltage Injuries

ANTHONY SANCES, JR., SENIOR MEMBER, IEEE, JOEL B. MYKLEBUST, MEMBER, IEEE, JOHN F. SZABLYA, FELLOW, IEEE, THOMAS J. SWIONTEK, MEMBER, IEEE, SANFORD J. LARSON, MICHAEL CHILBERT, THOMAS PRIETO, JOSEPH F. CUSICK, DENNIS J. MAIMAN, AND KARL PINTAR

Abstract—Studies were done in the hog with limb-to-limb contacts at potentials up to 2000 V. The current density in nerve, vessels, muscle, bone, fat, lungs, heart, kidney, liver, intestines, and spinal cord were determined. The current densities in the leg are largest in nerve and artery, followed by muscle, fat, and bone. The temperature was great-

est in fat and nerve. With forelimb-to-hindlimb current application, the current densities were largest in the back region. The spinal cord current density was approximately twice the average cross-sectional value.

INTRODUCTION

SINCE the first death due to commercial electrical current in 1879, electrical injury has become an increasingly serious world problem [1], [2]. The Consumer Product Safety Commission indicates that more than 2400 cases were seen in hospital emergency rooms in the United States during 1977. The National Center for Health Statistics estimates that for 1974-1976, 4 percent of the burns in the United States were electrically induced [3]. Similarly, the U.S. Army Institute of Surgical Research indicates that electrical burns comprised 3 percent of all thermal injuries over a 17 year period [4]. Although the effects of household voltages on biological subjects has been extensively investigated [2], [5], [6], little is known concerning the effects of distribution line potentials.

The contact voltage in powerline injuries is usually known; however, the currents and current pathways are difficult to reconstruct. Previous studies in the hog demonstrated limb-

Manuscript received May 12, 1982; revised August 27, 1982. This work was supported in part by the National Institute of General Medical Science under Grant R01 GM26956.

A. Sances, Jr., S. J. Larson, J. F. Cusick, and D. J. Maiman are with the Department of Neurosurgery, Medical College of Wisconsin, Milwaukee, WI 53226.

J. B. Myklebust is with the Neuroscience Research Laboratory, Veterans Administration Medical Center, Wood, WI 53193.

J. F. Szablya is with the Departments of Electrical Engineering and Environmental Sciences, Washington State University, Pullman, WA 99164.

T. J. Swiontek is with the Department of Electrical Engineering, Milwaukee School of Engineering, Milwaukee, WI 53233, and the Neuroscience Research Laboratory, Veterans Administration Medical Center, Wood, WI 53193.

M. Chilbert and T. Prieto are with the Department of Biomedical Engineering, Marquette University, Milwaukee, WI 53233.

K. Pintar is with the Department of Pathology, Medical College of Wisconsin, Milwaukee, WI 53226, and the Department of Laboratory Science, Veterans Administration Medical Center, Wood, WI 53193.